HOO radical scavenging activity of curcumin I and III in physiological conditions: a theoretical investigation on the influence of acid–base equilibrium and tautomerism†

Dinh Hieu Truong, [ab] Thi Tu Dinh,[cd] Thi My Duyen Trinh,[e] Thi Hong Minh Pham,[cd] Minh Quan Pham,[cd] Urszula Gawlik-Dziki[f] and Duy Quang Dao *[ab]

Curcumin possesses various effective medicinal properties, such as anti-cancer, anti-Alzheimer's, anti-inflammatory, and antioxidant effects, where its free radical scavenging activities play a crucial role in its therapeutic mechanisms. Although the antioxidant properties of curcumin and its derivatives have been previously studied, a systematic investigation of the thermodynamics and kinetics of the reaction with the hydroperoxide radical (HOO•) – a standardized free radical – in different solvents is lacking. This study examined the HOO• radical scavenging activities of two curcumin derivatives, specifically curcumin I (Cur-I) and curcumin III (Cur-III), in water and pentyl ethanoate (PEA) solutions using Density Functional Theory (DFT) approaches. The antioxidant properties of the neutral and anionic forms of their tautomers, including the keto–enol and diketone forms, were explored *via* three standard mechanisms: hydrogen abstraction (Abs), radical addition (Add), and single electron transfer (SET). Intrinsic parameters, thermochemical parameters, and kinetics of the curcumin-HOO• reactions were systematically characterized. As a result, the overall rate constant for the reaction of Cur-I in the water (9.36×10^7 M^{-1} s^{-1}) is approximately 3.6 times higher than that of Cur-III (2.60×10^7 M^{-1} s^{-1}). Meanwhile, the rate constants in PEA solvent are less significant, being 4.02×10^1 M^{-1} s^{-1} and 8.16×10^2 M^{-1} s^{-1} for Cur-I and Cur-III, respectively. Due to the dominant molar fraction of the keto–enol form compared to the diketone, the reaction rates are primarily attributed to the keto–enol form. The SET reaction of dianionic form contributes a decisive proportion to the overall rate constants of both Cur-I and Cur-III. Finally, an analysis of the chemical nature of the Abs reactions reveals that the most predominant hydrogen transfer at the phenolic −OH groups (*i.e.*, O22H and O23H) occurs *via* a proton-coupled electron transfer (PCET) mechanism.

1. Introduction

Curcumin, or 1,7-bis(4-hydroxy-3-methoxyphenyl)-1,6-heptadiene-3,5-dione, is the most prevalent naturally occurring polyphenol found in the roots of turmeric (*Curcuma longa* L.) and other Curcuma species. Curcuminoids, which

consist of curcumin, desmethoxycurcumin, and bisdesmethoxycurcumin,[1] are known for their diverse medicinal properties. Curcumin is an effective natural treatment exhibiting various medicinal activities, including anti-Alzheimer's disease,[2] anti-cancer,[3] anti-inflammatory,[4] antioxidant,[5] anti-microbial,[6] and anti-diabetic properties.[7]

Reactive free radicals are also believed to be one of the causes of inflammation, which is associated with several chronic diseases,[8] such as Alzheimer's disease, Parkinson's disease, cerebral injury, cardiovascular disease, metabolic disorders, and cancer. Furthermore, inflammation may be one of the primary contributors to the development of age-related diseases (*i.e.*, cancer, infections, inflammatory diseases).[9] Indeed, the neuroprotective effects of curcumin in inhibiting Alzheimer's disease (AD) through different mechanisms have widely been explored. Due to its free radical scavenging and anti-inflammation activities, curcumin has been observed to prevent and reduce cellular inflammation-related

[a]*Institute of Research and Development, Duy Tan University, Da Nang 550000, Vietnam. E-mail: daoduyquang@duytan.edu.vn*

[b]*School of Engineering and Technology, Duy Tan University, Da Nang 550000, Vietnam*

[c]*Graduate University of Science and Technology, Vietnam Academy of Science and Technology, Hanoi, Vietnam*

[d]*Institute of Natural Products Chemistry, Vietnam Academy of Science and Technology, Hanoi, Vietnam*

[e]*Faculty of Pharmacy, Duy Tan University, Da Nang 550000, Vietnam*

[f]*Department of Biochemistry and Food Chemistry, University of Life Sciences in Lublin, 8 Skromna St., 20-704 Lublin, Poland*

neurodegeneration and aging process[10] by binding to amyloid β peptide (Aβ) in the central nervous systems. Curcumin also has several potential properties in cancer treatment. Gupta *et al.* indicated that head and neck squamous cell carcinoma (HNSCC), myeloma, and colorectal cancer can be partially treated with curcumin.[11] The anti-cancer capabilities of curcumin are based on its capacity to induce apoptosis and reduce tumor proliferation and invasion by inhibiting several cellular signaling pathways. Curcumin is effective in treating both chronic and acute inflammation.[12] The anti-inflammatory properties of curcumin stem from its ability to inhibit neutrophil activity and the production of inflammatory prostaglandins derived from arachidonic acid.[12]

As mentioned above, several diseases originate from the reactivity of free radicals and/or transition metal ions. Consequently, the radical scavenging activities of curcumin have attracted considerable attention in the literature, using experimental and computational approaches. Numerous experimental studies have demonstrated the efficient antioxidant capacity of curcumin and its derivatives in preventing free radical damage in the human body.[13] The antioxidant properties of curcumin have been reported to be comparable to those of vitamins C and E.[14] Curcumin can eliminate and inactivate reactive nitrogen and oxygen species (RNS and ROS), as well as other free radicals and ROS-producing enzymes such as xanthine hydrogenase/oxidase and lipoxygenase/cyclooxygenase.[15] Additionally, the effects of curcumin on endothelial heme oxygenase-1 (HO-1) were investigated using cells from the bovine aortic endothelium. The results showed that curcumin enhances cellular resistance to oxidative damage after 18 h of incubation.[16]

Curcumin and its derivatives have also been the focus of various Density Functional Theory (DFT) studies in the literature.[17–24]

The reactivity of curcumin compounds has been predicted based on the evaluation of their electronic structures and the calculation of global quantum chemical indicators. Anjomshoa and coworkers investigated the effect of solvent on tautomerism, acidity, and radical stability of curcumin and some derivatives based on the thermodynamics parameters using B3LYP functional.[19] Results showed that the keto–enol form is significantly more stable than the diketone form in all studied solvents (*i.e.*, water, DMSO, acetonitrile, ethanol, acetone…). Manzanilla and Robles characterized the antioxidant properties of curcumin, caffeic acid phenethyl ester, and chicoric acid using the global chemical reactivity descriptors from conceptual DFT.[23] It is shown that both diketone and keto–enol forms of curcumin are weaker electron donors but better electron acceptors, making them effective anti-reductants according to the SET mechanism.

It is noteworthy that approaches based on the electronic properties, the quantum chemical descriptors, or intrinsic thermochemical parameters (*e.g.*, bond dissociation enthalpy (BDE), ionization potential (IP), proton affinity (PA), *etc.*) represent only the chemical nature of the studied compounds without considering the influence of reactive radical nature, or environment conditions. To address this issue, various computational studies have focused on the reactivity of curcumin towards different free radicals using thermodynamics and reaction kinetics analyses. For example, Sadatsharifi and Purgel (2021) evaluated the antiradical properties of alizarin and curcumin towards harmful small free radicals (*i.e.*, hydroxyl, peroxyl, and superoxide radicals) using the M06-2X/TZVP/SMD level of theory.[25] They explored all possible all possible autoxidation pathways through cyclic radical forms and showed that the key intermediate is the epoxide form, from which all cyclopentadione derivatives could be formed. Additionally, hydroxyketocyclopentadione and hemiacetalcyclopentadione were identified as the major oxidation products of curcumin. Anjomshoa *et al.* (2017) evaluated the radical-curcumin reactions with various reactive oxygen radicals (ROS), including $HO^{\bullet}$, $CH_3O^{\bullet}$, $HOO^{\bullet}$, and $O_2^{\bullet-}$, *via* four known mechanisms: SET, RAF, SPLET, and HAT, in water and *n*-octanol solutions by calculating standard Gibbs free energies (ΔG^0 at 298 K) using the BMK/6-311+G(d,p) level of theory.[18] The results showed that the HAT mechanism was consistently more dominant than RAF, SPLET, and SET. Furthermore, radical additions at the C1=C2 and C6=C7 double bonds are more favorable than at C3=C4 (Fig. 1). Other computational works on the thermodynamic properties of curcumin derivatives in the radical scavenging reactions.[26–30] However, these works were limited to the thermodynamic aspect and did not investigate the reaction kinetics.

Regarding the reaction kinetics of curcumin derivatives, there have been a limited number of experimental and computational studies. The reaction kinetics of curcumins with ROS were computationally investigated by Galano *et al.*[21] Specifically, they studied the influence of tautomerism and
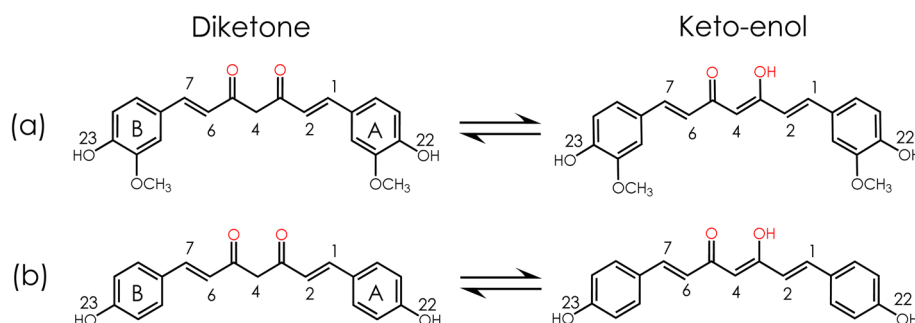

Fig. 1 Diketone and keto–enol tautomer structure of (a) Cur-I and (b) Cur-III.

acid–base equilibrium on the thermodynamics and kinetics of radical scavenging reactions (*i.e.*, 1,7-bis(4-hydroxy-3-methoxyphenyl)-1,6-heptadiene-3,5-dione, or Cur-I) toward methoxy radical ($CH_3O^\bullet$) in water and benzene solvents at the at the B3LYP/6-311+G(d,p) level of theory combined with the IEF-PCM solvent model.[21] The results showed that curcumin exists almost exclusively in its enol form in benzene solution, and in a ratio of 99.5% enol to 0.5% keto form in water. In terms of reaction kinetics, the reaction of Cur-I with $CH_3O^\bullet$ is governed by the HAT mechanism, which aligns with the experimental observations of Barclay *et al.*[31] The overall rate constants for the curcumin + $CH_3O^\bullet$ reaction were estimated to be 1.16×10^{10} and 5.52×10^9 L mol^{-1} s^{-1} in benzene and water, respectively. In water, the HAT mechanism was reported to be more predominant than the RAF one. Furthermore, Purushothaman *et al.* also predicted the rate constant of the reaction between Cur-I and HOO radical in the gas phase using the UB3LYP/6-311+G** level of theory,[27] and obtained a value of 1.9×10^{10} L mol^{-1} s^{-1}. Experimentally, Jovanovic *et al.* measured the reaction rate constant of Cur-I with the methyl radical being about $(3.5 \pm 0.3) \times 10^9$ L M^{-1} s^{-1}, which is close to diffusion control in 40% aqueous DMSO at pH of 5. The *tert*-butoxyl radical reacts with curcumin in acetonitrile solutions at a diffusion-controlled rate being $(7.5 \pm 0.8) \times 10^9$ L M^{-1} s^{-1}.[32] As can be seen, despite many attempts devoted to curcumin and its derivatives by experimental and computational approaches, there is still a need to systematically explore the reaction kinetics aspect of curcumin derivatives with HOO$^\bullet$, which is a standard ROS in several studies in literature, in various solvents, such as water and pentyl ethanoate (PEA).

Thus, this work aims to systematically evaluate the free radical scavenging activities of curcumin derivatives, including Cur-I (*i.e.*, monodemethoxycurcumin) and Cur-III (*i.e.*, bisdemethoxycurcumin), toward the HOO radical in two solvents with different polarities (*i.e.*, water and PEA). The geometrical and electronic structures of the keto–enol and diketone tautomers of each curcumin compound were first investigated. Three common antioxidant mechanisms were then studied, including hydrogen abstraction (Abs), radical addition (Add), and single electron transfer (SET). Different intrinsic parameters, including bond dissociation enthalpies (BDE), ionization potential (IP), and proton affinities (PA), were then calculated to quickly assess the antioxidant properties. Potential energy surfaces (PES) of the molecule-radical reactions were established. Additionally, the influence of the acid–base equilibrium and the tautomerism on the reaction rates of curcumin with HOO radicals was investigated in both solvents. The overall rate constants for curcumin-HOO radical reactions were also proposed, accounting for these influences. Finally, the chemical nature of hydrogen abstraction reactions was evaluated to distinguish whether it is a hydrogen atom transfer or a proton-coupled electron transfer (PCET) process.

2. Computational details

Gaussian 16 Revision C.01 package[33] was used for all calculations within the framework of Density Functional Theory. The geometrical and electronic structures, thermodynamics, and kinetics of the neutral and ionic species were investigated using the M06-2X functional,[34] combined with the 6-31+G(d,p) basis set.[35–37] The accuracy of the obtained energies was improved using the higher Pople basis set 6-311++G(3df,3pd). These computational approaches have been successfully applied to different molecular systems in recent studies.[38–40] A scaling factor of 0.952 was applied for the vibrational frequency calculations.[41] The influence of solvents, including water ($\varepsilon = 78.3553$) and pentyl pentanoate (PEA, $\varepsilon = 4.7297$), was modeled using the Solvation Model based on the quantum mechanical charge density of a solute molecule interacting with a continuum description of the solvent (SMD).[42] The conformational distribution of the studied compounds was scanned using the MSTor code.[43]

The influence of acid–base equilibrium on the HOO radical scavenging activities in the solvents was considered. In the lipid media, represented by the PEA solvent, all the studied compounds were assumed to exist in the neutral form. Conversely, in the polar environment (*i.e.*, water), three different deprotonation sites may exist in the hydroxyl or methylene groups (Fig. 1). The acid dissociation constants (pK_a) were computed using semi-empirical models proposed by Rebollar-Zepeda *et al.* for phenolic derivatives.[44] Details of the pK_a value and molar fraction of each existing form were presented in the ESI File.† The antioxidant mechanism and kinetics of the neutral and three anionic forms were then predicted *via* three standard processes: Abs, Add, and SET.

The pre-reactive complexes scheme proposed by Singleton and Cvetanovic[45] was used for the kinetic calculations of Abs and Add reactions. Details of calculation procedures can be found elsewhere.[38–40] Intrinsic reaction coordinate (IRC) calculations, using the Hessian-based predictor-corrector (HPC) integrator,[46–48] were performed to confirm whether the imaginary frequency corresponds to the appropriate motion along the reaction coordinates. The Gaussian Post Processor (GPOP) program[49] was used to compute the rate constants of all the reactions. The Gibbs free energy of activation of the SET reaction was computed based on Marcus's theory.[50–52] The apparent diffusion-corrected rate constant in the solvents was calculated using Collin–Kimball theory[53] and the steady-state Smoluchowski rate constant.[54]

Finally, the overall rate constants ($k_{overall}$) were calculated as the sum of the rate constant for Abs (k_{Abs}), Add (k_{Add}), and SET (k_{SET}) reactions, taking into account the molar fractions of each acid–base form and the respective tautomeric form *via* the following reactions (eqn (1)):

$$k_{overall} = F_{diketon} \times \sum_i f_i \times k_{tot}{}^i + F_{keto-enol} \times \sum_i f_i \times k_{tot}{}^i; \quad (1)$$

Here, i denotes the neutral, monoanionic, dianionic, and trianionic forms of curcumin I and III. k_{tot} represents the total rate constant for the three studied mechanisms (*i.e.*, Abs, Add, and SET), where $k_{tot} = k_{Abs} + k_{Add} + k_{SET}$. $F_{diketon}$ and $F_{keto-enol}$ are the molar fractions of the diketone and keto–enol forms of curcumin, respectively.

3. Results and discussion

3.1. Structure and electronic properties

Fig. 2 shows the optimized geometry and electronic structure of the most stable diketone and keto–enol tautomers of Cur-I and Cur-III in water; the ones in PEA are displayed in Fig. S1 (ESI File).†

In terms of geometrical structure, the diketone tautomer exhibits a V-shaped structure with the methylene group (–CH$_2$–) at the center, while the keto–enol tautomer adopts a quasi-planar form, favoring strong delocalization of electron densities. Both Cur-I and Cur-III contain two phenolic –OH groups, which may act as hydrogen-donating sites. Additionally, the methylene group of the diketone tautomer may serve as a radical attack site *via* the Abs process. The diketone form possesses two double bonds, whereas the keto–enols forms have three double bonds, which are the reactive sites for Add reactions.

Regarding the distribution of frontier orbitals, the HOMO and LUMO are primarily located at C=C bonds and phenyl rings, indicating their potential involvement in the Add reaction. In the ESP map, the most negative atomic regions of the diketone tautomer are found at the C=O groups and phenyl rings. Meanwhile, the most negative regions in the keto–enol tautomer are spread throughout the entire molecular molecule chain. Conversely, the most positive atomic regions are concentrated around the phenolic –OH and –OCH$_3$ functional groups.

3.2. Intrinsic thermochemical parameters

Table 1 presents several intrinsic thermochemical properties, including bond dissociation enthalpies (BDE), proton affinity (PA), and ionization potential (IP) of the diketone and keto–enol tautomers of Cur-I and Cur-III in water and PEA. Cartesian coordinates, optimized structures, and thermochemical data for the diketone and keto–enol tautomers of Cur-I and Cur-III in water and PEA are summarized in Table S1 of the ESI File.†

All the studied compounds favorably dissociate, forming anionic species and donating protons in water. The PA values are notably lower than the BDE and IP ones. For example, for Cur-I compounds, the lowest PA values of the diketone in water are 124.1, 128.0, and 129.5 kJ mol^{-1} at the C4H, O22H, and O23H positions, respectively. Meanwhile, the lowest BDE values of this compound are 354.8, 357.3, and 389.3 kJ mol^{-1} at the O22H, O23H, and C4H positions, respectively.

Similarly, for the keto–enol form in water, the lowest PA values are found at the phenolic hydroxyl groups, with values of 131.4 (O23H), 132.2 (O22H), and 135.2 kJ mol^{-1} (O20H), while its lowest BDE is significantly higher: 351.3 (O23H), 351.5 (O22H), and 364.5 kJ mol^{-1} (O20H). The IP is substantially
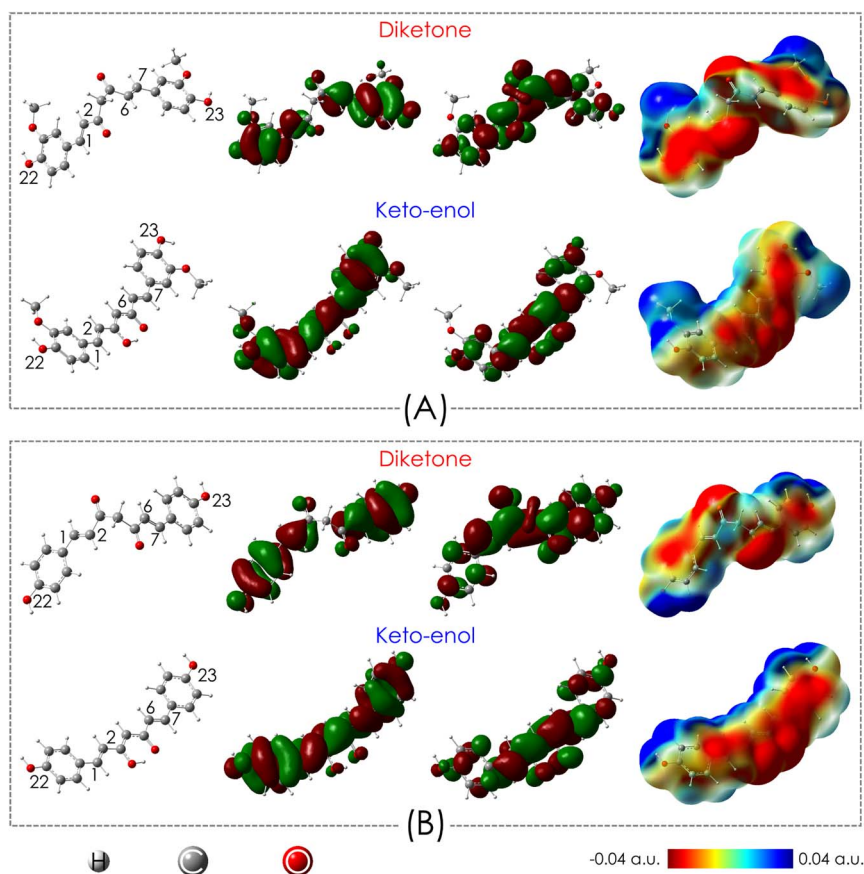

Fig. 2 Optimized geometries, HOMO, LUMO and ESP maps of diketone and keto–enol tautomers of Cur-I (A) and Cur-III (B) in water.

Table 1 The BDE, PA, and IP of the diketone and keto–enol tautomers of Cur-I and Cur-III (unit in kJ mol^{-1})

| Position | Cur-I | | | | | | Cur-III | | | | | |
| | Diketone | | | Keto–enol | | | Diketone | | | Keto–enol | | |
	BDE	PA	IP	BDE	PA	IP	BDE	PA	IP	BDE	PA	IP
Water												
—			527.4			518.5			543.6			528.9
O22H	357.3	128.0		351.5	**131.4**		**374.9**	129.1		**368.3**	133.0	
O23H	**354.8**	129.5		**351.3**	132.2		**374.9**	129.1		371.8	**132.6**	
O20H	—	—		464.5	135.2		—	—		463.0	137.1	
C1H	—	292.6		—	—		—	307.0		—	—	
C2H	—	234.5		—	—		—	223.7		—	—	
C4H	389.3	**124.1**		464.9	293.1		388.5	**124.4**		495.5	293.6	
C6H	—	212.6		—	—		—	223.7		—	—	
C7H	—	302.2		—	—		—	307.2		—	—	
C24H	421.1	—		421.4	—		—	—		—	—	
C25H	419.0	—		421.0	—		—	—		—	—	
PEA												
—			536.6			550.8			579.8			560.4
O22H	356.1	250.7		352.3	**250.3**		**365.7**	**239.9**		362.6	240.4	
O23H	**353.5**	251.9		**351.7**	252.9		**365.7**	**239.9**		**360.0**	**239.7**	
O20H	—	—		463.3	283.4		—	—		462.2	283.1	
C1H	—	411.4		—	—		—	420.3		—	—	
C2H	—	367.4		—	—		—	366.7		—	—	
C4H	384.0	**248.1**		490.1	418.3		384.1	247.8		490.0	418.0	
C6H	—	354.2		—	—		—	366.7		—	—	
C7H	—	412.6		—	—		—	420.3		—	—	
C24H	415.6	—		415.7	—		—	—		—	—	
C25H	416.2	—		416.0	—		—	—		—	—	

higher than both the PA and the BDE, with 527.4 for the diketone and 518.5 kJ mol^{-1} for the keto–enol.

Thus, the diketone and keto–enol forms of Cur-I may readily donate protons through three steps, each characterized by different acid dissociation constants (pK_a values), as presented in the next section. Similar trends are observed for the Cur-III in both tautomeric forms. The antioxidant properties of the studied compounds in water depend on the activities of their anionic forms. The lower PA values, in comparison to the BDE and IP, suggest that proton transfer and electron transfer either sequentially or in a coupled manner, may be dominant processes. This observation is consistent with findings in lipid media.

3.3. Acid–base equilibria

Acid–base equilibria play a crucial role in the free radical scavenging activities of the potential antioxidant compounds. We computed the acid dissociation constants (pK_a) for three proton dissociation steps for all the studied curcumins in the aqueous phase. As a result, the three most favored deprotonation sites for each compound are shown in Table S2 (ESI).† The pK_a values for the three dissociation steps of the diketone form are 7.1, 8.9, and 9.2 for Cur-I and 7.3, 8.8, and 9.2 for Cur-III. The corresponding values of the keto–enol form are 7.9, 8.7, and 9.0 for Cur-I and 7.9, 9.0, and 9.1 for Cur-III. These values are in good agreement with the experimental ones measured for the curcumin mixture (7.9, 8.5, and 9.0).[55]

Fig. S1 (ESI)† shows the evolution of the molar fraction for the different forms of the studied compounds. It can be observed that under acidic conditions (pH below 7.0), the diketone and keto–enol tautomers of Cur-I and Cur-III are predominantly present in their neutral and monoanionic forms. However, under basic conditions (pH above 7.0), further deprotonations occur, resulting in the presence of not only the neutral and monoanion forms but also the dianionic and trianionic forms. Table S3 (ESI)† summarizes the molar fraction of the co-existing forms at physiological pH (7.4).

At physiological conditions, the diketone form of Cur-I, for example, predominantly exists in the monoanion form (63.44%) in the aqueous phase, followed by the neutral form (34.54%), with smaller proportions of the dianion (1.99%) and trianion (0.33%). Meanwhile, its keto–enol tautomer is mostly present in the neutral form (75.10%), with lesser amounts of monoanion (23.78%), dianion (1.09%), and trianion (0.03%). Similar trends are observed for the Cur-III.

To fully understand the antioxidant activity of Cur-I and Cur-III, all forms – neutral, monoanion, dianion, and trianion – of both tautomers will be evaluated in their reactions with the HOO radical in water.

3.4. Free radical scavenging mechanism

3.4.1. HOO˙ free radical scavenging mechanism of Cur-I. Fig. S2 (ESI)† presents the optimized transition states (TS) structures for the Abs reactions at the phenolic –OH groups in

water and PEA, as well as the Add reactions at various carbon centers of the double bonds in the neutral and monoanionic forms of the diketone of Cur-I. Cartesian coordinates of all the reactant complexes (RC), TS, and product complexes (PC) for the Abs and Add reactions between Cur-I and HOO radical calculated in water and PEA are provided in Table S4 (ESI File).†

For the abstraction reactions, the bond distances between the (HOO)O⋯H(HO–) fluctuate between 1.36–1.39 Å in water and 1.31–1.32 Å in PEA, while the –O⋯H bond lengths of the phenolic hydroxyl group are approximately 1.06–1.07 Å in water and 1.09–1.10 Å in PEA. The O–H–O bond angles are about 160–161°. For the addition reactions, the interactive lengths between C⋯O(HOO) range from 1.90–2.01 Å in water and around 1.93–1.97 Å in PEA.

Fig. 3 shows the ZPE-corrected relative enthalpy profile at 0 K (ΔH_{0K}) for the Abs and Add reactions of the Cur-I in water and PEA. In water, the monoanion (MoA) of the diketone and the neutral (Neu) form of the keto–enol tautomer are chosen as representative cases due to their highest molar fractions (63.44 and 75.10%, Table S3, ESI†). The potential energy surfaces (PES)

of other neutral and anionic forms are presented in Table S5 (ESI).†

The Abs reaction between the MoA diketone and the radical occurs primarily at the phenolic O22H and O23H groups in four steps: reactant complexes (RC), transition states (TS), product complexes (PC), and separated products (RAD), with similar relative enthalpy profiles at 0 K (ΔH_{0K}). The ΔH_{0K} values for the TS are 29.4 and 29.5 kJ mol^{-1} for TS22 and TS23, respectively, while the product enthalpies (RAD22 and RAD23) are −26.8 and −27.5 kJ mol^{-1}. Regarding the Neu keto–enol, the most favorable Add reaction is found at the C4 with the ΔH_{0K} value being 18.3 kJ mol^{-1}.

The Add process takes place in three consecutive steps: RC, TS, and PC. Five Add reactions are observed at the C1, C2, C4, C6, and C7 positions of the MoA diketone. The Add reaction of HOO radical at the C4 position is found to be the most predominant, with the lowest TS enthalpy value of 18.3 kJ mol^{-1} (TS4) and the most negative product enthalpy (PC4, −48.2 kJ mol^{-1}). In contrast, the Add processes at C1 and C7, near the phenolic rings, show the highest TS enthalpies of 45.0
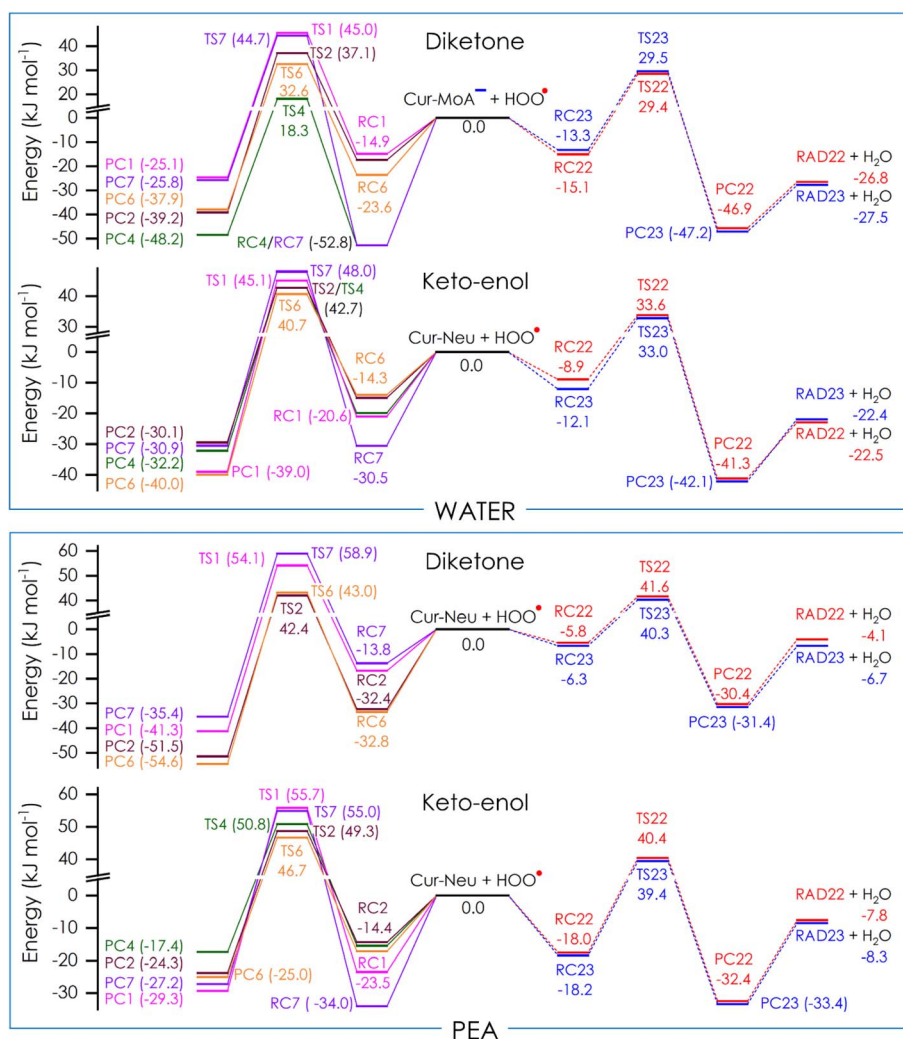

Fig. 3 ZPE-corrected relative enthalpy profile at 0 K (ΔH_{0K}) for abstraction (right) and addition (left) reactions initiated by HOO• radical of Cur-I in water and PEA.

(TS1) and 44.7 kJ mol^{-1} (TS7). For the Neu keto–enol, the lowest Add TS is found at the C6 with a TS enthalpy value of 40.7 kJ mol^{-1} (TS6).

Thus, it is noteworthy that regarding the MoA diketone, the Add reaction is more predominant than the Abs one (18.3 kJ mol^{-1} of TS4 compared to 29.4 kJ mol^{-1} of TS22), while in the Neu keto–enol, the reverse observation is found (40.7 kJ mol^{-1} of TS6 compared to 33.0 kJ mol^{-1} of TS22).

The Neu keto–enol tautomer exhibits lower free radical scavenging activity than the MoA diketone, with higher TS and product enthalpies. For example, the ΔH_{0K} values for the TS22 and TS23 in the Abs reaction are 33.0 and 33.6 kJ mol^{-1}, respectively, higher than those for the MoA diketone (29.4 and 29.5 kJ mol^{-1}), while the product enthalpies (RAD22 and RAD23) are −22.5 and −22.4 kJ mol^{-1}, respectively (Fig. 3). Similarly, the most predominant Add reaction is observed at the C6 position, with higher relative enthalpies for TS6 (40.7 kJ mol^{-1}) and PC6 (−40.0 kJ mol^{-1}).

In PEA solvent (a lipid-like medium), both tautomers are present in their neutral form, and their radical scavenging activities are less favorable than in the aqueous phase. For instance, the relative enthalpies of TS22 and TS23 for the Abs reactions of the neutral diketone are 41.6 and 40.3 kcal mol^{-1}, respectively, which are about 10 kcal mol^{-1} higher than those in water. Similar values of 41.6 and 40.3 kcal mol^{-1} are observed for the TS22 and TS23 of the neutral keto–enol tautomer. A similar trend is recognized for the Add processes in PEA (Fig. 3).

3.4.2. HOO$^\bullet$ free radical scavenging of Cur-III. The optimized structures of the transition states (TSs) for the Abs and Add reaction of Cur-III in the diketone and keto–enol forms with the HOO radical in water and PEA are shown in Fig. S3 (ESI).† We present the TS structures of MoA for the diketone and the Neu form for the keto–enol tautomer, which represent the most significant molar fractions in the aqueous phase, *i.e.*, 54.38% and 77.56%, respectively (Table S3, ESI†). The structures of other anionic forms are shown in Table S1 (ESI).† In contrast, only the Neu form of both the tautomers is present in the PEA solvent.

As shown in Fig. S3 (ESI),† the −O···H bond lengths of the phenolic hydroxyl group range from approximately 1.08 to 1.11
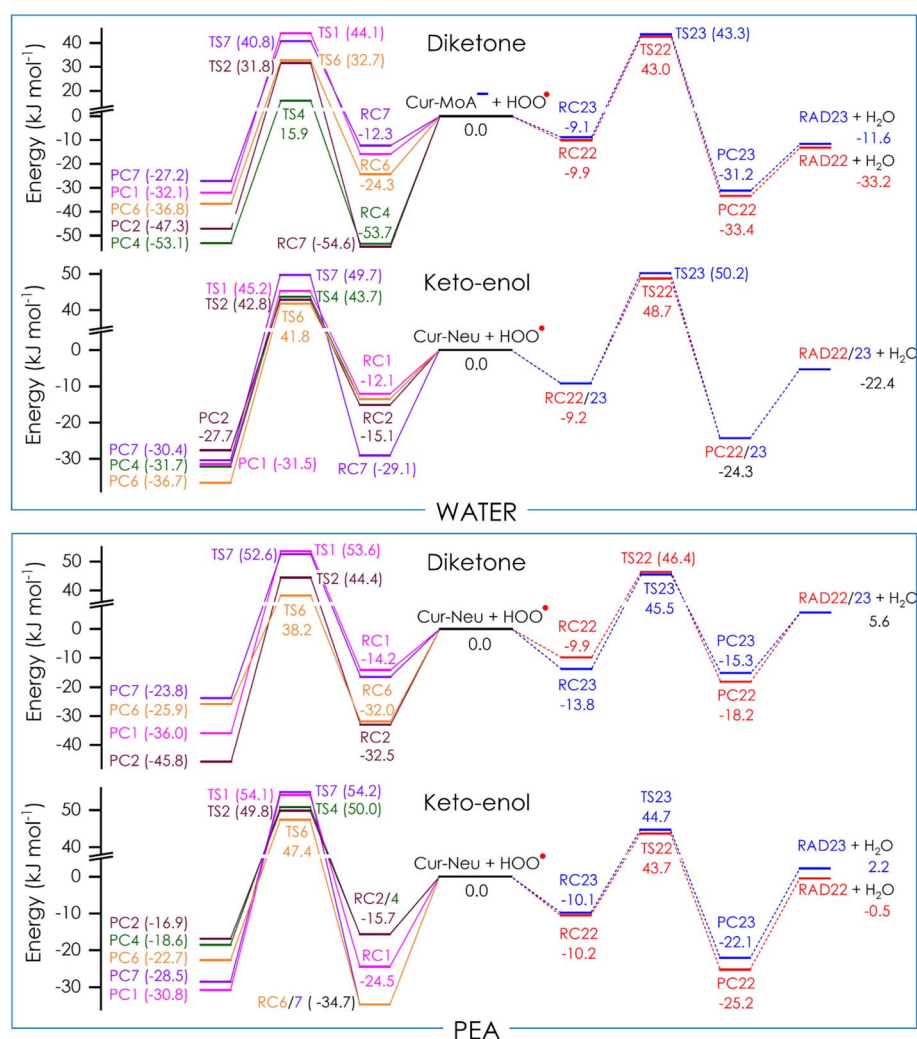

Fig. 4 ZPE-corrected relative enthalpy profile at 0 K (ΔH_{0K}) for abstraction (right) and addition (left) reactions initiated by HOO$^\bullet$ radical of Cur-III in water and PEA.

Å for the Abs reactions at the O22H and O23H positions in water, while in PEA, they range from 1.11 to 1.12 Å. The (HOO) O⋯H(HO–) distances range from 1.27 to 1.32 Å for the Abs reactions in water and from 1.26 to 1.27 Å in PEA. The O–H–O bond angles vary between 163 and 165° in both media. For the Add processes, the C⋯O(HOO) interaction distances range from 1.93 to 2.04 Å in water and from 1.93 to 1.96 Å in PEA.

The ZPE-corrected relative enthalpy profiles at 0 K for the reactions of Cur-III and HOO radicals in water and PEA are shown in Fig. 4. Cartesian coordinates of all the RC, TS, and PC for the Abs and Add reactions between Cur-III and HOO radical calculated in water and PEA are provided in Table S4 (ESI File).†

Firstly, it is noteworthy that the Add reaction of HOO radical is more favorable than the Abs for both the MoA diketone and Neu keto–enol form of the Cur-III. Indeed, the most favorable reaction of the MoA diketone is the Add at C4 position (TS4, 15.9 kJ mol^{-1}), and the most predominant one of the Neu keto–enol is also the Add at C6 position (TS6, 41.8 kJ mol^{-1}) (Fig. 4).

Additionally, comparing the reactivities between the Neu keto–enol and MoA diketone, the Neu keto–enol displays a lower radical scavenging activity than the MoA diketone. In fact, the Abs reactions of the Neu keto–enol exhibit higher relative enthalpy values for TS (ΔH_{0K} of 48.7 and 50.2 kJ mol^{-1} for TS22 and TS23, respectively) compared to those of the MoA diketone tautomer (43.0 and 43.3 kJ mol^{-1}). The lowest relative enthalpy for the TS of the Add reaction of the Neu keto–enol (41.8 kJ mol^{-1} for TS6) is also higher than that of the MoA diketone (15.9 kJ mol^{-1} for TS4).†

The potential energy surfaces (PES) of other neutral and anionic forms of both Cur-I and Cur-III in the aqueous phase are presented in Table S5 (ESI).† Briefly, by observing the PESs of other existing forms for the diketone (neutral, dianionic, and trianionic forms), and the ones for the keto–enol (monoanionic, dianionic, and trianionic forms), it is observed that the HOO radical scavenging activities in the aqueous phase of Cur-I are always higher than the ones of Cur-III. For example, the lowest ΔH_{0K} value for TS of the Neu diketone of Cur-I is 34.0 kJ mol^{-1} (TS22 and TS6), which is smaller than the ones of Neu diketone of Cur-III being 34.2 kJ mol^{-1} (TS6). Furthermore, the Add reaction is observed to be more favorable than the Abs one for all the species presented in Table S5 (ESI).†

In PEA, the TSs of Abs reaction for the diketone tautomer show higher relative enthalpies (46.4 and 45.5 kJ mol^{-1} for TS22 and TS23, respectively) compared to the keto–enol (43.7 and 44.7 kJ mol^{-1}). Conversely, the Add reaction for the diketone has a lower ΔH_{0K} value for TS than the Neu keto–enol. The lowest ΔH_{0K} value for the diketone is observed in the reaction at C6 (TS6, 38.2 kJ mol^{-1}), which is lower than that of the keto–enol (TS6, 47.4 kJ mol^{-1}). Furthermore, the Add is observed to be more favorable than the Abs for the MoA diketone, while a reverse finding is observed for the Neu keto–enol.

Thus, comparing the relative enthalpy profiles of the diketone and keto–enol forms, the observations are similar for the Cur-I and Cur-III. In water, the radical addition reaction to double bonds is more favorable than the hydrogen abstraction one. In addition, the diketone tautomer exhibits higher antioxidant activities than the keto–enol one. However, the overall

activities of each tautomer are also depending on the molar fractions of the neutral and anionic species. In PEA, the Neu diketone exhibits higher relative enthalpies for the Abs TS but lower relative enthalpies for the Add TS compared to the Neu keto–enol.

In the next section, the kinetic aspect will be explored to provide further evidence of the influence of tautomerism and acid–base equilibrium on the radical scavenging activities of Cur-I and Cur-III.

3.5. Kinetics of reactions

The reaction kinetics between the neutral and anionic forms of the diketone and keto–enol compounds were calculated to enable a more accurate prediction of their free radical scavenging activities. We investigated three standard free radical-molecule mechanisms: Abs, Add, and SET, in both water and PEA solvents. The Add and Abs reactions are typical one-step mechanisms, which often occur concurrently depending on the molecular structure of the antioxidant. The potential for the Add mechanism to occur is influenced by the antioxidant's structure, particularly the presence of multiple bonds, which are favorably positioned to interact with free radical. Additionally, the Abs plays a critical role in the activity of many organic antioxidants, especially phenolic compounds in their neutral form. As a result, the relative significance of the Abs mechanism is strongly affected by the properties of the reactive environment, such as pH and polarity.[56]

In contrast, the SET process serves as a critical step in two-step mechanisms such as single electron transfer followed by proton transfer (SET-PT) and sequential proton loss electron transfer (SPL-ET) mechanism, where electron transfer is either preceded or followed by proton transfer to achieve a more stable, lower-energy state. In polar environments like water, proton transfer is assumed to occur rapidly, making the SET step pivotal in determining the overall reaction rate of the process.[57] The efficiency of the SET process depends on the electron-donating ability of the antioxidant and the electron-accepting nature of the free radical.

Accordingly, the three antioxidant mechanisms, including Abs, Add, and SET, have been extensively studied within antioxidant research. For this investigation, the Gibbs free energy of activation ($\Delta G^{\ddagger}$, kJ mol^{-1}) and Gibbs free energy of reaction ($\Delta_r G^0$, kJ mol^{-1}), thermal rate constant (k_T, M^{-1} s^{-1}), diffusion rate constant (k_D, M^{-1} s^{-1}), and apparent rate constant (k_{app}, M^{-1} s^{-1}) were calculated for the diketone and keto–enol forms of Cur-I (Tables S6† and 2) and Cur-III (Tables S7† and 3). The apparent rate constants were subsequently adjusted based on the molar fractions of Cur-I and Cur-III, yielding corrected rate constants (k_{app}^{Mf}, M^{-1} s^{-1}), respectively. Herein, we only present in Tables 2 and 3 the corresponding results obtained from the keto–enol forms due to its predominant molar fractions.

Table S6† summarizes the kinetics parameters of all the reactions between the diketone form of Cur-I and the HOO radical in PEA and water. Generally, the antioxidant reactivity of Cur-I varies significantly depending on the acid–base equilibrium. In water, the Neu and MoA forms primarily react with the

Table 2 The Gibbs free energy of activation ($\Delta G^{\ddagger}$, kJ mol^{-1}) and reaction ($\Delta_r G^0$, kJ mol^{-1}), thermal rate constant (k_T, M^{-1} s^{-1}), diffusion rate constant (k_D, M^{-1} s^{-1}), apparent rate constant (k_{app}, M^{-1} s^{-1}), apparent rate constant corrected by the molar fraction of Cur-I (k_{app}^{Mf}, M^{-1} s^{-1}), and branching ratio (Γ, %) for the reactions between HOO$^{\bullet}$ radical and the keto–enol tautomer of Cur-I in water and PEA at 298 K

Form	Position	$\Delta G^{\ddagger}$	$\Delta_r G^0$	k_T	k_D	k_{app}	k_{app}^{Mf}	Γ
Water								
Neutral (f_i = 75.10%)	**Abstraction reaction**							
	O22H	−25.5	80.1	4.01×10^3	2.42×10^9	4.01×10^3	3.01×10^3	0.00
	O23H	−23.0	78.8	5.14×10^3	2.42×10^9	5.14×10^3	3.86×10^3	0.00
	Addition reaction							
	C1	8.9	88.6	7.83×10^{-2}	2.00×10^9	7.83×10^{-2}	5.88×10^{-2}	0.00
	C2	16.5	90.3	3.66×10^{-2}	2.01×10^9	3.66×10^{-2}	2.52×10^{-2}	0.00
	C4	11.9	89.0	5.12×10^{-2}	1.97×10^9	5.12×10^{-2}	3.85×10^{-2}	0.00
	C6	9.2	86.0	1.89×10^{-1}	2.01×10^9	1.89×10^{-1}	1.42×10^{-1}	0.00
	C7	17.2	91.9	2.16×10^{-2}	1.97×10^9	2.16×10^{-2}	1.62×10^{-2}	0.00
	Single electron transfer reaction							
		142.6	174.3	4.46×10^{-17}	8.45×10^9	4.46×10^{-17}	3.44×10^{-17}	0.00
MonoAnion (f_i = 23.78%)	**Abstraction reaction**							
	O22H	−29.5	74.4	1.57×10^4	2.42×10^9	1.57×10^4	3.72×10^3	0.00
	O23H	−29.7	72.8	2.06×10^4	2.42×10^9	2.06×10^4	4.90×10^3	0.01
	Addition reaction							
	C1	21.5	88.4	7.85×10^{-2}	2.01×10^9	7.85×10^{-2}	1.87×10^{-2}	0.00
	C2	4.1	78.3	3.85×10^0	2.03×10^9	3.85×10^0	9.14×10^{-1}	0.00
	C4	−4.2	66.9	3.17×10^2	1.92×10^9	3.17×10^2	7.54×10^1	0.00
	C6	−2.6	79.0	3.23×10^0	2.04×10^9	3.23×10^0	7.68×10^{-1}	0.00
	C7	8.8	88.7	7.03×10^{-2}	2.08×10^9	7.03×10^{-2}	1.67×10^{-2}	0.00
	Single electron transfer reaction							
		66.7	66.7	2.91×10^2	8.48×10^9	2.91×10^2	6.91×10^1	0.00
DiAnion (f_i = 1.09%)	**Abstraction reaction**							
	O23H	11.8	75.5	1.78×10^4	2.39×10^9	1.78×10^4	1.95×10^2	0.00
	Addition reaction							
	C1	20.4	86.9	1.48×10^{-1}	2.03×10^9	1.48×10^{-1}	1.62×10^{-3}	0.00
	C2	−8.1	55.6	4.95×10^4	2.25×10^9	4.95×10^4	5.42×10^2	0.00
	C4	−12.0	62.8	1.67×10^3	1.90×10^9	1.67×10^3	1.83×10^1	0.00
	C6	7.0	78.8	3.18×10^0	2.00×10^9	3.18×10^0	3.48×10^{-2}	0.00
	C7	14.8	88.3	8.30×10^{-2}	1.98×10^9	8.30×10^{-2}	9.08×10^{-4}	0.00
	Single electron transfer reaction							
		3.2	16.0	2.35×10^{11}	8.62×10^9	8.31×10^9	9.10×10^7	97.60
TriAnion (f_i = 0.03%)	**Addition reaction**							
	C1	20.4	87.2	1.23×10^{-1}	2.05×10^9	1.23×10^{-1}	3.24×10^{-5}	0.00
	C2	−7.4	55.0	6.75×10^4	2.26×10^9	6.75×10^4	1.77×10^1	0.00
	C4	2.7	61.9	2.41×10^3	1.89×10^9	2.41×10^3	6.32×10^{-1}	0.00
	C6	−1.3	54.0	5.87×10^4	2.24×10^9	5.87×10^4	1.54×10^1	0.00
	C7	21.4	85.3	2.51×10^{-1}	2.01×10^9	2.51×10^{-1}	6.59×10^{-5}	0.00
	Single electron transfer reaction							
		0.4	13.9	5.57×10^{11}	8.58×10^9	8.45×10^9	2.22×10^6	2.38
Total							9.32×10^7	100.00
Pentyl ethanoate								
Neutral (f_i = 100.00%)	**Abstraction reaction**							
	O22H	−6.32	89.55	1.91×10^1	2.63×10^9	1.91×10^1	1.91×10^1	47.54
	O23H	−6.30	88.88	2.11×10^1	2.66×10^9	2.11×10^1	2.11×10^1	52.45
	Addition reaction							
	C1	18.31	102.37	2.95×10^{-4}	2.17×10^9	2.95×10^{-4}	2.95×10^{-4}	0.00
	C2	28.01	98.46	1.33×10^{-3}	2.18×10^9	1.33×10^{-3}	1.33×10^{-3}	0.00
	C4	33.44	98.48	1.19×10^{-3}	2.14×10^9	1.19×10^{-3}	1.19×10^{-3}	0.00
	C6	20.40	96.43	2.88×10^{-3}	2.16×10^9	2.88×10^{-3}	2.88×10^{-3}	0.00
	C7	27.10	107.52	4.20×10^{-5}	2.16×10^9	4.20×10^{-5}	4.20×10^{-5}	0.00
Total							4.02×10^1	100.00

HOO radical *via* the Abs reaction at the O22H and O23H positions, as well as the Add reactions at the C4 atom. In contrast, for the dianion (DiA) and trianion (TriA) forms, the favorable mechanism involves the SET process. The Abs reactions at O22H and O23H yield diffusion-corrected apparent rate constants (k_{app}^{Mf}) of 1.45×10^3 and 2.63×10^3 M^{-1} s^{-1} for the Neu form, and 2.31×10^4 and 3.80×10^3 M^{-1} s^{-1} for the MoA. For the MoA, the Add reaction at the C4 position has a rate

Table 3 The Gibbs free energy of activation ($\Delta G^{\ddagger}$, kJ mol^{-1}) and reaction ($\Delta_r G^0$, kJ mol^{-1}), thermal rate constant (k_T, M^{-1} s^{-1}), diffusion rate constant (k_D, M^{-1} s^{-1}), apparent rate constant (k_{app}, M^{-1} s^{-1}), apparent rate constant including the molar fraction of Cur-III (k_{app}^{Mf}, M^{-1} s^{-1}), and branching ratio (Γ, %) for the reactions between the HOO$^{\bullet}$ radical and the keto–enol tautomer of Cur-III in water and PEA at 298 K

Form	Position	$\Delta G^{\ddagger}$	$\Delta_r G^0$	k_T	k_D	k_{app}	k_{app}^{Mf}	Γ
Water								
Neutral (f_i = 77.56%)	**Abstraction reaction**							
	O23H	−6.1	88.4	8.31×10^2	2.43×10^9	8.31×10^2	6.44×10^2	0.00
	O22H	−6.1	88.1	9.73×10^2	2.42×10^9	9.73×10^2	7.54×10^2	0.00
	Addition reaction							
	C1	14.0	89.4	5.84×10^{-2}	2.05×10^9	5.84×10^{-2}	4.53×10^{-2}	0.00
	C2	18.9	89.8	4.18×10^{-2}	2.05×10^9	4.18×10^{-2}	3.24×10^{-2}	0.00
	C4	11.8	87.4	9.74×10^{-2}	2.01×10^9	9.74×10^{-2}	7.55×10^{-2}	0.00
	C6	11.2	87.3	1.13×10^{-1}	2.05×10^9	1.13×10^{-1}	8.76×10^{-2}	0.00
	C7	16.5	97.2	2.59×10^{-3}	2.01×10^9	2.59×10^{-3}	2.01×10^{-2}	0.00
	Single electron transfer reaction							
		127.7	135.9	2.36×10^{-10}	8.28×10^9	2.36×10^{-10}	1.83×10^{-10}	0.00
MonoAnion (f_i = 21.92%)	**Abstraction reaction**							
	O23H	−11.2	77.1	2.23×10^4	2.14×10^9	2.23×10^4	4.89×10^3	0.02
	O22H	−11.2	77.0	2.30×10^4	2.14×10^9	2.30×10^4	5.39×10^3	0.02
	Addition reaction							
	C1	15.6	90.4	3.52×10^{-2}	2.03×10^9	3.52×10^{-2}	7.73×10^{-3}	0.00
	C2	9.9	81.1	1.26×10^0	2.06×10^9	1.26×10^0	2.27×10^{-1}	0.00
	C4	−4.3	68.2	1.93×10^2	1.94×10^9	1.93×10^2	4.23×10^1	0.00
	C6	9.9	81.1	1.23×10^0	2.06×10^9	1.23×10^0	2.70×10^{-1}	0.00
	C7	17.4	91.1	3.04×10^{-2}	2.06×10^9	3.04×10^{-2}	6.66×10^{-3}	0.00
	Single electron transfer reaction							
		69.5	69.6	9.56×10^1	8.33×10^9	9.56×10^1	2.10×10^1	0.00
DiAnion (f_i = 0.51%)	**Abstraction reaction**							
	O23H	−14.4	81.1	3.41×10^4	2.04×10^9	3.41×10^4	1.73×10^2	0.00
	Addition reaction							
	C1	20.4	86.9	1.48×10^{-1}	2.03×10^9	1.48×10^{-1}	1.62×10^{-3}	0.00
	C2	−8.1	55.6	4.95×10^4	2.25×10^9	4.95×10^4	5.42×10^2	0.00
	C4	−12.0	62.8	1.67×10^3	1.90×10^9	1.67×10^3	1.83×10^1	0.00
	C6	7.0	78.8	3.18×10^0	2.00×10^9	3.18×10^0	3.48×10^{-2}	0.00
	C7	14.8	88.3	8.30×10^{-2}	1.98×10^9	8.30×10^{-2}	9.08×10^{-4}	0.00
	Single electron transfer reaction							
		16.1	23.2	1.30×10^{10}	8.33×10^9	5.08×10^9	2.57×10^7	98.70
TriAnion (f_i = 0.01%)	**Addition reaction**							
	C1	21.8	76.6	8.16×10^0	2.05×10^9	8.16×10^0	8.20×10^{-4}	0.00
	C2	1.2	57.6	1.32×10^4	2.19×10^9	1.32×10^4	1.30×10^0	0.00
	C4	−1.1	61.4	2.95×10^3	1.92×10^9	2.95×10^3	2.90×10^{-1}	0.00
	C6	1.5	60.8	3.58×10^3	2.15×10^9	3.58×10^3	3.51×10^{-1}	0.00
	C7	16.1	80.7	1.71×10^0	2.09×10^9	1.71×10^0	1.68×10^{-4}	0.00
	Single electron transfer reaction							
		11.8	25.3	5.52×10^9	8.40×10^9	3.33×10^9	3.27×10^5	1.26
Total							2.61×10^7	100.00
Pentyl ethanoate								
Neutral (f_i = 100.00%)	**Abstraction reaction**							
	O22H	−3.7	85.7	4.61×10^2	2.68×10^9	4.61×10^2	4.61×10^2	56.52
	O23H	−0.8	86.4	3.55×10^2	2.68×10^9	3.55×10^2	3.55×10^2	43.48
	Addition reaction							
	C1	14.3	98.1	1.66×10^{-3}	2.23×10^9	1.66×10^{-3}	1.66×10^{-3}	0.00
	C2	27.3	95.3	4.54×10^{-3}	2.21×10^9	4.54×10^{-3}	4.54×10^{-3}	0.00
	C4	24.8	92.9	1.13×10^{-2}	2.20×10^9	1.13×10^{-2}	1.13×10^{-2}	0.00
	C6	21.4	93.6	9.07×10^{-3}	2.22×10^9	9.07×10^{-3}	9.07×10^{-3}	0.00
	C7	20.1	102.4	3.25×10^{-4}	2.21×10^9	3.25×10^{-4}	3.25×10^{-4}	0.00
Total							8.16×10^2	100.00

constant of 1.44×10^3 M^{-1} s^{-1}. However, these mechanisms become negligible for the DiA and TriA forms, where the SET process dominates, with rate constants of 1.60×10^8 and 2.65×10^6 M^{-1} s^{-1}, respectively.

Regarding the branching ratio (Γ, %), although the DiA and TriA forms of Cur-I diketone represent only 1.99 and 0.03%, their SET reactions contribute substantially, with branching ratios of 98.35% and 1.63% of the overall rate constant,

respectively. In PEA solvent, the Abs reactions at the –O22H and –O23H positions are the predominant processes, with rate constants of 1.50×10^1 M^{-1} s^{-1} (Γ, 27.95%) and 3.85×10^1 M^{-1} s^{-1} (Γ, 71.87%), respectively.

Similar observations apply to the keto–enol tautomer of Cur-I in both water and PEA (Table 2). In water, the Abs is the predominant process for the Neu and MoA forms, with rate constants of $3.01 \times 10^3/3.86 \times 10^3$ M^{-1} s^{-1} and $3.72 \times 10^3/4.90 \times 10^3$ M^{-1} s^{-1}, respectively, for the O22H/O23H abstraction reactions, while the Add and the SET processes are negligible. In contrast, the SET becomes the dominant reaction for the DiA and TriA forms, with rate constants of 9.10×10^7 and 2.22×10^6 M^{-1} s^{-1}, respectively, corresponding to Γ values of 97.60% and 2.38% of the total rate constant for Cu-I in the aqueous phase. Additionally, in the PEA environment, Abs reactions at –O22H (1.91×10^1 M^{-1} s^{-1}, 47.54%) and –O23H (2.11×10^1 M^{-1} s^{-1}, 52.45%) are more significant than the Add ones.

Notably, the rate constants for the diketone tautomers in water are higher than those of the keto–enol compound, while the opposite trend is observed in the PEA solvent. Specifically, the total rate constant of the diketone in water is 1.62×10^8 M^{-1} s^{-1}, exceeding that of the keto–enol at 9.32×10^7 M^{-1} s^{-1}. In PEA, however, the total rate constant for the diketone is 1.36×10^1 M^{-1} s^{-1}, which is lower than that of the keto–enol at 4.02×10^1 M^{-1} s^{-1}.

Tables S7† and 3 present the kinetic results for HOO radical scavenging reactions of the diketone and the keto–enol tautomers of Cur-III in water and PEA solvents.

The relative antioxidant activity between the diketone and keto–enol forms differs for Cur-III compared to Cur-I. In the aqueous phase, the Neu and MoA forms of the diketone generally exhibit higher rate constants for the Abs reactions than the keto–enol tautomer. Specifically, the rate constants for the Abs reaction at O22H/O23H positions are $1.13 \times 10^3/1.46 \times 10^3$ M^{-1} s^{-1} for the Neu diketone (Table S7†), higher than those the Neu keto–enol at $6.44 \times 10^2/7.54 \times 10^2$ M^{-1} s^{-1} (Table 3). For the MoA forms, the rate constants are $5.82 \times 10^3/3.03 \times 10^3$ M^{-1} s^{-1} for the diketone, compared to $4.89 \times 10^3/5.39 \times 10^3$ M^{-1} s^{-1}, for the keto–enol. Additionally, the Add reaction at the C4 position of the MoA diketone shows a significant rate constant of 1.02×10^3 M^{-1} s^{-1}, contributing substantially to the

total rate constant, whereas that of the MoA keto–enol is much lower at only 4.23×10^1 M^{-1} s^{-1}.

Furthermore, the SET mechanism also plays a key role in the antioxidant activities of Cur-III, particularly for the DiA and TriA forms. The DiA and TriA forms of both the diketone and the keto–enol tautomers primarily react with the HOO radical via SET reactions, similar to what is observed in Cur-I compounds. The SET rate constants of the DiA and TriA diketone are 1.82×10^6 and 1.27×10^5 M^{-1} s^{-1} (Table S7, ESI†), respectively, both lower than those for the keto–enol, at 2.57×10^7 and 3.27×10^5 M^{-1} s^{-1} (Table 3). Additionally, the SET of MoA form significantly contributes to the overall rate constant of the diketone, with a value of 3.47×10^3 M^{-1} s^{-1} (Table S7†). Thus, the higher total rate constant of the keto–enol form (2.61×10^7 M^{-1} s^{-1}) compared to that of the diketone (1.96×10^6 M^{-1} s^{-1}) is largely due to the high SET rate constant of its DiA form (2.57×10^7 M^{-1} s^{-1}). As in the case of Cur-I, the SET process of the DiA and TriA forms makes a substantial contribution to the overall rate constant of Cur-III in water, despite their low molar fractions.

In PEA solvent, the abstraction reactions at the O22H/O23H positions are the most predominant, with rate constants of $1.01 \times 10^3/1.11 \times 10^2$ M^{-1} s^{-1} for the diketone tautomer, and $4.61 \times 10^2/3.55 \times 10^2$ M^{-1} s^{-1} for the keto–enol. Meanwhile, the Add and SET processes are negligible. Additionally, the total rate constant of the diketone in PEA (1.12×10^3 M^{-1} s^{-1}, Table S7†) is higher than that of the keto–enol (8.16×10^2 M^{-1} s^{-1}, Table 3).

Finally, Table 4 summarizes the total apparent rate constants of the diketone and keto–enol tautomers, as well as the overall rate constants of Cur-I and Cur-III, taking into account the molar fraction of each tautomer in both the aqueous phase and the PEA solvent.

It is noteworthy that the keto–enol tautomer of both Cur-I and Cur-III is the most predominant form, with molar fractions ranging from 99.4% to 99.9%, consistent with finding by Galano et al. (Galano et al., 2009).[21] For this reason, although the apparent rate constants (k_{app}) of the diketone tautomer are higher than those of the keto–enol form, the total rate constants corrected by molar fraction (k_{Mf}) for the keto–enol tautomer are consistently higher than those for the diketone in both water and PEA solvent. Specifically, in water, the k_{Mf} value for the

Table 4 The apparent diffusion-corrected rate constant (k_{app}, M^{-1} s^{-1}), the molar fraction of each tautomer form (Mf, %), the total rate constant of each tautomer considering its molar fraction (k_{Mf}, M^{-1} s^{-1}), and its corresponding branching ratio (Γ, %) for the reactions between the HOO• and Cur-I and Cur-III in water and PEA at 298 K

Tautomers	Water				PEA			
	k_{app}	Mf	k_{Mf}	Γ	k_{app}	Mf	k_{Mf}	Γ
Cur-I								
Diketone	1.62×10^8	0.59	9.53×10^5	1.02	5.36×10^1	0.01	7.14×10^{-3}	0.02
Keto–enol	9.32×10^7	99.41	9.26×10^7	98.98	4.02×10^1	99.99	4.02×10^1	99.98
Overall			$\mathbf{9.36 \times 10^7}$	**100.00**			$\mathbf{4.02 \times 10^1}$	**100.00**
Cur-III								
Diketone	1.96×10^6	0.14	2.81×10^3	0.01	1.12×10^3	0.20	2.26×10^0	0.28
Keto–enol	2.61×10^7	99.86	2.60×10^7	99.99	8.15×10^2	99.80	8.14×10^2	99.72
Overall			$\mathbf{2.60 \times 10^7}$	**100.00**			$\mathbf{8.16 \times 10^2}$	**100.00**

keto–enol form of Cur-I is 9.26×10^7 M^{-1} s^{-1}, accounting for 98.98% of the total rate constant, which is nearly 100 times greater than that of the diketone (9.53×10^5 M^{-1} s^{-1}, representing only 1.02%). In PEA, the k_{Mf} for the keto–enol is 4.02×10^1 M^{-1} s^{-1}, about 1000 times higher than that of the keto–enol (7.14×10^{-3} M^{-1} s^{-1}). A similar trend is observed with Cur-III. Comparing the overall rates of Cur-I and Cur-III, we find that in water, the overall rate constant of Cur-I (9.36×10^7 M^{-1} s^{-1}) is approximately 3.6 times higher than that of Cur-III (2.60×10^7 M^{-1} s^{-1}); however, the reverse is observed in PEA, where Cur-I has a rate constant of 4.02×10^1 M^{-1} s^{-1} compared to 8.16×10^2 M^{-1} s^{-1} for Cur-III.

Compared to other results reported in the literature on curcumin derivatives, our calculated total rate constant for Cur-I with the HOO radical in water (9.36×10^7 M^{-1} s^{-1}) is comparable to experimental observation with CCl$_3$O$_2$ radical ($(7.10 \pm 0.2) \times 10^7$ M^{-1} s^{-1}), ascorbic acid ($(2.80 \pm 0.1) \times 10^7$ M^{-1} s^{-1}),[28] as well as with the computational data for the CH$_3$O radical in water ($(7.39 \pm 0.8) \times 10^8$ M^{-1} s^{-1}).[21] Additionally, our computed result is about 100 times lower than the experimental rate constant for the *tert*-butoxyl radical (7.50×10^9 M^{-1} s^{-1}) in a 40% aqueous DMSO at pH 5,[32] yet approximately 100 times higher than the experimental measurement with O$_2$$^{•-}$ ($(2.70 \pm 0.3) \times 10^5$ M^{-1} s^{-1}).[28] It is also around 10^4 times higher than computational data of Cur-I with HOO radical in the gas phase (1.90×10^4 M^{-1} s^{-1}).[27] The differences in rate constants are primarily due to the distinct reactivities of the free radicals involved.

It is evident that the tautomerism significantly influences the reaction kinetics of both Cur-I and Cur-III, with the keto–enol form playing a decisive role due to its high molar fraction. This predominance of the keto–enol tautomer can be attributed to its molecular structure (Fig. 2). Specifically, the keto–enol form features a highly conjugated π-system with three C=C double bonds along the linker and two aromatic rings, allowing both HOMO and LUMO orbitals to distribute across the entire molecule, thereby stabilizing the keto–enol structure. In contrast, the diketone form has a central –C4H$_2$– group, which disrupts the conjugation within the π-system, limiting HOMO and LUMO distribution to the molecular extremities and resulting in a higher formation energy than that of the keto–enol form.

Furthermore, the acid–base equilibrium also presents a significant impact on the reaction kinetics in solutions. In water, the higher rate constant of Cur-I compared to Cur-III (9.36×10^7 M^{-1} s^{-1} and 2.60×10^7, M^{-1} s^{-1}, respectively; Table 4) is primarily due to the significantly SET rate constant of the dianion (DiA) form of Cur-I (9.10×10^7 M^{-1} s^{-1}; Table 2) compared to that of Cur-III (2.57×10^7 M^{-1} s^{-1}; Table 3). This difference can be attributed to the electron-donating effect of the *o*-methoxy phenolic groups in the DiA form of Cur-I's keto–enol structure, which increases electron density at the neighboring anionic O$^-$ position. This effect likely enhances the electron-donating capability of the DiA form of Cur-I keto–enol toward the HOO radical, facilitating the SET reaction. The essential role of the SET process in the antioxidant activities of

phenolic compounds, especially in anionic forms, has been widely documented in the literature.[58–60]

In contrast, in PEA solvent, both Cur-I and Cur-III exist primarily in the neutral form, where the electron-donating effect of two *o*-methoxyl substituents is less conducive to the hydrogen-donating process. Additionally, in Cur-I, the formation of hydrogen bonds between the –OH and –OCH$_3$ groups stabilizes the molecular structure, making hydrogen donation from the –OH substituents more difficult than in Cur-III, which contains lone –OH groups without additional stabilization. As a result, the rate constant of Cur-I (4.02×10^1 M^{-1} s^{-1}) is lower than that of Cur-III (8.06×10^2 M^{-1} s^{-1}).

3.6. Is hydrogen abstraction a HAT or PCET process?

In the context of the hydrogen transfer process, several reaction mechanisms can occur within the complex biological environment, influenced by various factors. Both concerted mechanisms (*i.e.*, hydrogen atom transfer, HAT, or proton-coupled electron transfer, PCET) or sequential mechanisms (*i.e.*, sequential proton loss-electron transfer, SPL-ET, or sequential electron transfer-proton transfer, SET-PT)[61,62] may be involved. While the sequential processes are distinguished by thermodynamic parameters associated with the formation of different intermediates, like radical anions or radical cations, differentiating concerted mechanisms is more challenging.

Both HAT and PCET processes originate from similar reactants and lead to the same products, making them indistinguishable based solely on thermodynamic criteria. The distinction between these two processes lies in how charged particles (*i.e.*, electron and proton) are transferred. In HAT, the electron and proton are transferred together along the same pathway, while in PCET, they are transferred independently from different reactive sites of the donor molecule (DH) to the acceptor molecule (AH).

Several computational approaches have been developed to distinguish HAT from PCET, including: (i) analysis of the atomic charge and spin density of DH, AH, and the transferred hydrogen along the intrinsic reaction coordinates (IRC) of the hydrogen transfer reaction, and (ii) analysis of the singly occupied molecular orbital (SOMO).

Fig. 5 illustrates the distributions of singly occupied molecular orbitals (SOMO) for the transition states (TS) and the evolution of spin densities and Natural Population Analysis (NPA) atomic charges for hydrogen donor (DH), hydrogen (H) and hydrogen acceptor (AH) along the intrinsic reaction coordinates (IRC) for the predominant hydrogen abstraction processes at O22H and O23H positions (Abs-O22H and Abs-O23H) of Cur-I and Cur-III compounds in the aqueous phase.

The SOMO distributions at the transition state of the hydrogen transfer reaction are generally regarded as reliable indicators for distinguishing between HAT and PCET processes.[63–66] Typically, for a HAT reaction, the SOMO of the TS exhibits a high atomic orbital density aligned along the hydrogen transition vector, with a nodal plane positioned at the hydrogen species' location. In contrast, for the PCET process, the SOMO of the TS comprises p orbitals that are orthogonal to
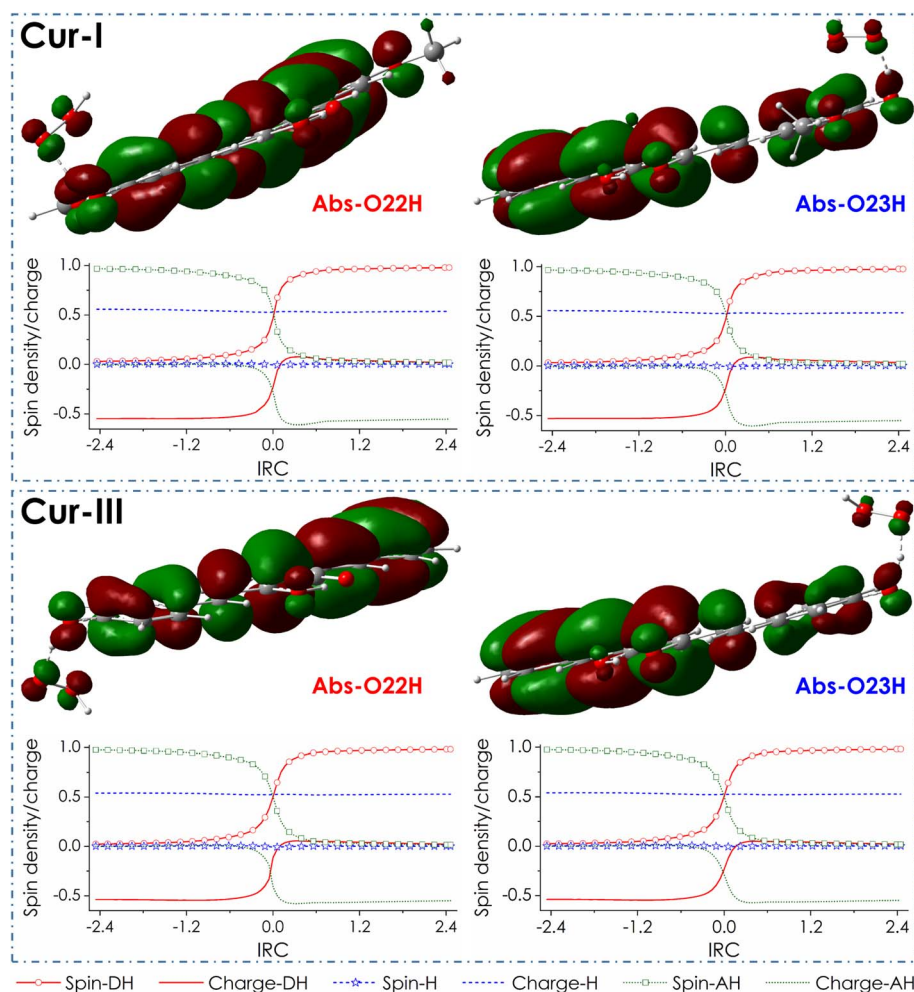
Fig. 5 Evolutions of spin and Natural Population Analysis (NPA) atomic charges for hydrogen donor (DH), hydrogen (H), and hydrogen acceptor (AH) along the intrinsic reaction coordinates (IRC) for the predominant hydrogen abstraction processes at O22H and O23H positions (Abs-O22H and Abs-O23H) of Cur-I and Cur-III compounds in the aqueous phase. The singly occupied molecular orbitals (SOMO) for the transition states (TSs) of each reaction, computed with the iso-density value of 0.02 a.u. are also presented.

the transition vector. Based on these indicators, as shown in Fig. 5, the most prominent TS for the abstraction reaction of Cur-I demonstrates a bent angle of approximately 120° to 150° between the p orbital of the oxygen species in the hydrogen donor (DH) and that of the hydrogen acceptor (AH). A similar observation is noted for the abstraction reactions of Cur-III. This finding serves as the first indication that the studied process may involve hydrogen transfer.

Conversely, in the reaction at the O22H of Cur I, the charge on the transferred hydrogen species remains approximately 0.53–0.55e, indicating that it likely corresponds to a positively charged proton. Meanwhile, the charge of the DH, represented by the oxygen species of Cur-I, increases from about −0.55e to a peak value of 0.07e before stabilizing at a value close to zero (*i.e.*, 0.02e). One of the AH exhibits a decrease from 0 to a minimum of −0.61e, followed by a slight increase to about −0.55e upon separation of the hydrogen from the DH. Additionally, the spin density of transferred hydrogen remains consistently zero along the IRC. In contrast, the spin density of

the DH increases significantly from 0.02 to 0.98, while the spin density of the AH decreases from 0.97 to 0.02 as the HOO radical forms a bond with the hydrogen species. A similar phenomenon

Table 5 Natural electron configuration (NEC) for the hydrogen species (H), hydrogen donor (DH), and hydrogen acceptor (AH, or HOO radical) analyzing at the transition state of the most dominant hydrogen transfer processes of Cur-I and Cur-III towards HOO radical in an aqueous environment

CurI-O22H	H	$1S^0$
	O-DH	$[Core]2S^{1.65}2p^{5.06}$
	O-AH	$[Core]2S^{1.82}2p^{4.58}$
CurI-O23H	H	$1S^0$
	O-DH	$[Core]2S^{0.83}2p^{2.47}$
	O-AH	$[Core]2S^{0.91}2p^{2.12}$
CurIII-O22H	H	$1S^0$
	O-DH	$[Core]2S^{0.83}2p^{2.42}$
	O-AH	$[Core]2S^{0.90}2p^{2.24}$
CurIII-O23H	H	$1S^0$
	O-DH	$[Core]2S^{0.83}2p^{2.42}$
	O-AH	$[Core]2S^{0.90}2p^{2.20}$

is observed in the reaction at the O23H position of Cur-I and in the reactions at both the O22H and O23H positions of Cur-III.

Finally, a Natural Electron Configuration (NEC) analysis is conducted for the H, DH, and AH species at the transition states of the Abs reaction (Table 5). All the hydrogen species involved exhibit a $1S^0$ electron configuration, indicating the chemical structure of a proton. In addition, both DH and AH display 2p orbital of the oxygen species. These observations confirm that the transferred hydrogen species is indeed a proton, which participates in a proton-coupled electron transfer (PCET) process.

4. Conclusions

The scavenging reactions of the HOO radical by two curcumin derivatives, namely curcumin I (Cur-I) and curcumin III (Cur-III), were evaluated in aqueous and pentyl ethanoate (PEA) solutions using Density Functional Theory DFT at the M06-2X/6-311++G(3df,3pd)//M06-2X/6-31+G(d,p) level of theory. Several intrinsic parameters, including bond dissociation energy (BDE), ionization potential (IP), and proton affinity (PA), along with thermochemical parameters of the reactions ($\Delta_r G^0$ and $\Delta G^‡$ at 298 K), and reaction kinetics, were systematically calculated to predict three standard antioxidant processes, hydrogen abstraction (Abs), radical addition followed by fragmentation (Add), and single electron transfer (SET). The contribution of the tautomerism and acid–base equilibria in the solutions to the overall rate constants was characterized in detail by considering reactions for both keto–enol and diketone forms, as well as the neutral, monoanionic, dianionic, and trianionic forms of two curcumin derivatives. The conclusions drawn from this analysis are as follows:

(i) Cur-I and Cur-III predominantly exist in the keto–enol tautomer form, with molar fraction of 99.4 and 99.9%, respectively. Concurrently, both curcumin derivatives are primarily present in the neutral and monoanionic forms, with molar fractions ranging from 98 to 99%. In contrast, the dianionic and trianionic forms account for only 1.0 to 2.0% in aqueous solution.

(ii) In aqueous solution, the reactions of the neutral and monoanionic forms primarily proceed *via* the Abs process at the phenolic hydroxyl groups (O22H and O23H), rather than through Add and SET pathways. In contrast, SET processes dominate the reactions of the dianionic and trianionic forms. Among these, the SET reactions of the dianionic form play a crucial role, with branching ratio values up to 98.70%/92.71% for the keto–enol form and 97.60%/98.35% for the diketone form of the Cur-I and Cur-III, respectively. Notably, despite their low molar fractions, the dianionic and trianionic forms make the most significant contributions to the reactions of both curcumin derivatives.

(iii) In PEA, the Abs reactions at the phenolic hydroxyl groups (O22H and O23H) are, as expected, the most predominant pathways for both tautomers of Cur-I and Cur-III derivatives, with branching ratios close to 100%.

(iv) Since the keto–enol tautomer is the most dominant form for both Cur-I and Cur-III, it contributes around 98–99% to the overall reaction rates. The rate constants for the keto–enol form in water are $9.26 \times 10^7\ M^{-1}\ s^{-1}$ and $2.60 \times 10^7\ M^{-1}\ s^{-1}$ for Cur-I and Cur-II, respectively. In the PEA, the rate constants are significantly lower, at 4.02×10^1 and $8.14 \times 10^2\ M^{-1}\ s^{-1}$, respectively.

(v) The overall rate constants for the reactions in water are 9.36×10^7 for Cur-I and $2.60 \times 10^7\ M^{-1}\ s^{-1}$ for Cur-III. In contrast, the rate constants in PEA are significantly lower, at $4.02 \times 10^1\ M^{-1}\ s^{-1}$ for Cur-I and $8.06 \times 10^2\ M^{-1}\ s^{-1}$ for Cur-III. Due to the presence of two *o*-methoxyl phenolic groups, Cur-I exhibits a higher rate constant in water compared to Cur-III, attributed to the electron-donating effects of the CH_3O groups to the anionic O^- positions, which favor the SET reaction of the dianionic form of Cur-I. However, in the PEA solution where both Cur-I and Cur-III are present in the neutral form, Cur-III shows higher rate constants than Cur-I due to the formation of hydrogen bonds between the –OH and $–OCH_3$ groups.

(vi) Analyses of the SOMO orbitals, atomic charges, spin densities along the intrinsic reaction coordinate (IRC), and Natural Electron Configuration (NEC) reveal that all the hydrogen transfer processes proceed *via* a proton-coupled electron transfer (PCET) mechanism.

This computational study provides a systematic perspective on the radical scavenging activities of curcumin derivatives, highlighting the influence of key factors such as acid–base equilibrium and tautomerism on reaction rates. The findings also have broader implications for the potential medicinal applications of curcumin derivatives.

Data availability

Data will be made available on request.

Author contributions

Dinh Hieu Truong: investigation, formal analysis, data curation. Thi Tu Dinh: investigation, formal analysis, data curation. Thi My Duyen Trinh: investigation, formal analysis, data curation. Thi Hong Minh Pham: formal analysis, data curation, writing – review & editing. Minh Quan Pham: formal analysis, writing – review & editing. Urszula Gawlik-Dziki: formal analysis, supervision, writing – review & editing. Duy Quang Dao: writing – original draft, investigation, formal analysis, data curation, supervision.

Conflicts of interest

The authors declare that they have no known competing financial interests or personal relationships that could have appeared to influence the work reported in this article.

Acknowledgements

References

1 A. Duvoix, R. Blasius, S. Delhalle, M. Schnekenburger, F. Morceau, E. Henry, M. Dicato and M. Diederich, *Cancer Lett.*, 2005, **223**, 181–190.

2 G. P. Lim, T. Chu, F. Yang, W. Beech, S. A. Frautschy and G. M. Cole, *J. Neurosci.*, 2001, **21**, 8370–8377.

3 A. Mukhopadhyay, C. Bueso-Ramos, D. Chatterjee, P. Pantazis and B. B. Aggarwal, *Oncogene*, 2001, **20**, 7597–7609.

4 D. Perrone, F. Ardito, G. Giannatempo, M. Dioguardi, G. Troiano, L. Lo Russo, A. De Lillo, L. Laino and L. Lo Muzio, *Exp. Ther. Med.*, 2015, **10**, 1615–1623.

5 T. Masuda, T. Maekawa, K. Hidaka, H. Bando, Y. Takeda and H. Yamaguchi, *J. Agric. Food Chem.*, 2001, **49**, 2539–2547.

6 P. S. Negi, G. K. Jayaprakasha, L. Jagan Mohan Rao and K. K. Sakariah, *J. Agric. Food Chem.*, 1999, **47**, 4297–4300.

7 N. Arun and N. Nalini, *Plant Foods Hum. Nutr.*, 2002, **57**, 41–52.

8 L. Lao, J.-H. Cui, M. Gerla and D. Maggiorini, in *Proceedings IEEE INFOCOM 2006. 25TH IEEE International Conference on Computer Communications*, IEEE, Barcelona, Spain, 2006, pp. 1–6.

9 E. S. Cannizzo, C. C. Clement, R. Sahu, C. Follo and L. Santambrogio, *J. Proteomics*, 2011, **74**, 2313–2323.

10 T. L. Moore, B. G. E. Bowley, P. L. Shultz, S. M. Calderazzo, E. J. Shobin, A. R. Uprety, D. L. Rosene and M. B. Moss, *Somatosens. Mot. Res.*, 2018, **35**, 1–10.

11 S. C. Gupta, S. Patchva and B. B. Aggarwal, *AAPS J.*, 2013, **15**, 195–218.

12 A. Mukhopadhyay, N. Basu, N. Ghatak and P. K. Gujral, *Agents Actions*, 1982, **12**, 508–515.

13 A. Ramirez-Boscá, A. Soler, M. A. Carrión Gutierrez, J. Laborda Alvarez and E. Quintanilla Almagro, *AGE*, 1995, **18**, 167–169.

14 K. I. Priyadarsini, D. K. Maity, G. H. Naik, M. S. Kumar, M. K. Unnikrishnan, J. G. Satav and H. Mohan, *Free Radical Biol. Med.*, 2003, **35**, 475–484.

15 V. P. Menon and A. R. Sudheer, in *The Molecular Targets and Therapeutic Uses of Curcumin in Health and Disease*, ed. B. B. Aggarwal, Y.-J. Surh and S. Shishodia, Springer US, Boston, MA, 2007, vol. 595, pp. 105–125.

16 R. Motterlini, R. Foresti, R. Bassi and C. J. Green, *Free Radical Biol. Med.*, 2000, **28**, 1303–1312.

17 I. O. Alisi, A. Uzairu and S. E. Abechi, *Bull. Natl. Res. Cent.*, 2020, **44**, 137.

18 S. Anjomshoa, M. Namazian and M. R. Noorbala, *Theor. Chem. Acc.*, 2017, **136**, 103.

19 S. Anjomshoa, M. Namazian and M. R. Noorbala, *J. Solution Chem.*, 2016, **45**, 1021–1030.

20 Y. Boulmokh, K. Belguidoum, F. Meddour and H. Amira-Guebailia, *Struct. Chem.*, 2024, **35**, 825–839.

21 A. Galano, R. Álvarez-Diduk, M. T. Ramírez-Silva, G. Alarcón-Ángeles and A. Rojas-Hernández, *Chem. Phys.*, 2009, **363**, 13–23.

22 R. Hazarika and B. Kalita, *Struct. Chem.*, 2021, **32**, 1701–1715.

23 B. Manzanilla and J. Robles, *J. Mol. Model.*, 2022, **28**, 68.

24 C. G. Vera-de La Garza, R. J. Martinez and F. Belmont-Bernal, *Struct. Chem.*, 2023, **34**, 1427–1438.

25 M. Sadatsharifi and M. Purgel, *J. Mol. Model.*, 2021, **27**, 166.

26 S. Biswas and P. K. Shukla, *Mol. Simul.*, 2023, **49**, 589–598.

27 A. Purushothaman, K. S. Teena Rose, J. M. Jacob, R. Varatharaj, K. Shashikala and D. Janardanan, *Food Chem.*, 2022, **373**, 131499.

28 S. A. M. Shaikh, B. G. Singh, A. Barik, N. V. Balaji, G. V. Subbaraju, D. B. Naik and K. I. Priyadarsini, *J. Mol. Struct.*, 2019, **1193**, 166–176.

29 L. Shen and H.-F. Ji, *Spectrochim. Acta, Part A*, 2007, **67**, 619–623.

30 Y.-M. Sun, H.-Y. Zhang, D.-Z. Chen and C.-B. Liu, *Org. Lett.*, 2002, **4**, 2909–2911.

31 L. R. C. Barclay, M. R. Vinqvist, K. Mukai, H. Goto, Y. Hashimoto, A. Tokunaga and H. Uno, *Org. Lett.*, 2000, **2**, 2841–2843.

32 S. V. Jovanovic, S. Steenken, C. W. Boone and M. G. Simic, *J. Am. Chem. Soc.*, 1999, **121**, 9677–9681.

33 M. J. Frisch, G. W. Trucks, H. B. Schlegel, G. E. Scuseria, M. A. Robb, J. R. Cheeseman, G. Scalmani, V. Barone, G. A. Petersson, H. Nakatsuji, X. Li, M. Caricato, A. V. Marenich, J. Bloino, B. G. Janesko, R. Gomperts, B. Mennucci, H. P. Hratchian, J. V. Ortiz, A. F. Izmaylov, J. L. Sonnenberg, Williams, F. Ding, F. Lipparini, F. Egidi, J. Goings, B. Peng, A. Petrone, T. Henderson, D. Ranasinghe, V. G. Zakrzewski, J. Gao, N. Rega, G. Zheng, W. Liang, M. Hada, M. Ehara, K. Toyota, R. Fukuda, J. Hasegawa, M. Ishida, T. Nakajima, Y. Honda, O. Kitao, H. Nakai, T. Vreven, K. Throssell, J. A. Montgomery Jr, J. E. Peralta, F. Ogliaro, M. J. Bearpark, J. J. Heyd, E. N. Brothers, K. N. Kudin, V. N. Staroverov, T. A. Keith, R. Kobayashi, J. Normand, K. Raghavachari, A. P. Rendell, J. C. Burant, S. S. Iyengar, J. Tomasi, M. Cossi, J. M. Millam, M. Klene, C. Adamo, R. Cammi, J. W. Ochterski, R. L. Martin, K. Morokuma, O. Farkas, J. B. Foresman and D. J. Fox, *Gaussian 16 Rev. C.01*, 2016.

34 Y. Zhao and D. G. Truhlar, *Theor. Chem. Acc.*, 2008, **120**, 215–241.

35 D. Feller, *J. Comput. Chem.*, 1996, **17**, 1571–1586.

36 B. P. Pritchard, D. Altarawy, B. Didier, T. D. Gibson and T. L. Windus, *J. Chem. Inf. Model.*, 2019, **59**, 4814–4820.

37 K. L. Schuchardt, B. T. Didier, T. Elsethagen, L. Sun, V. Gurumoorthi, J. Chase, J. Li and T. L. Windus, *J. Chem. Inf. Model.*, 2007, **47**, 1045–1052.

38 D. Q. Dao, S. Taamalli, F. Louis, D. Kdouh, Z. Srour, T. C. Ngo, D. H. Truong, V. Fèvre-Nollet, M. Ribaucour,

A. El Bakali and I. Černušák, *Chemosphere*, 2023, **312**, 137234.

39 H. K. Al Rawas, R. Al Mawla, T. Y. N. Pham, D. H. Truong, T. L. A. Nguyen, S. Taamalli, M. Ribaucour, A. El Bakali, I. Černušák, D. Q. Dao and F. Louis, *Environ. Sci.: Processes Impacts*, 2023, **25**, 2042–2056.

40 T. C. Ngo, S. Taamalli, Z. Srour, V. Fèvre-Nollet, A. El Bakali, F. Louis, I. Černušák and D. Q. Dao, *J. Environ. Chem. Eng.*, 2023, **11**, 109941.

41 I. M. Alecu, J. Zheng, Y. Zhao and D. G. Truhlar, *J. Chem. Theory Comput.*, 2010, **6**, 2872–2887.

42 A. V. Marenich, C. J. Cramer and D. G. Truhlar, *J. Phys. Chem. B*, 2009, **113**, 6378–6396.

43 W. Chen, J. Zheng, J. L. Bao, D. G. Truhlar and X. Xu, *Comput. Phys. Commun.*, 2023, **288**, 108740.

44 A. M. Rebollar-Zepeda, T. Campos-Hernández, M. T. Ramírez-Silva, A. Rojas-Hernández and A. Galano, *J. Chem. Theory Comput.*, 2011, **7**, 2528–2538.

45 D. L. Singleton and R. J. Cvetanovic, *J. Am. Chem. Soc.*, 1976, **98**, 6812–6819.

46 *Theory and Applications of Computational Chemistry: The First Forty Years*, ed. C. E. Dykstra, Elsevier, Amsterdam; Boston, 1st edn, 2005.

47 H. P. Hratchian and H. B. Schlegel, *J. Chem. Theory Comput.*, 2005, **1**, 61–69.

48 H. P. Hratchian and H. B. Schlegel, *J. Chem. Phys.*, 2004, **120**, 9918–9924.

49 A. Miyoshi, *GPOP Software*, rev. 2022.01.20m1, 2022, available from the author. See http://akrmys.com/gpop/. http://akrmys.com/gpop/.

50 R. A. Marcus, *J. Chem. Phys.*, 1957, **26**, 872–877.

51 R. A. Marcus, *J. Chem. Phys.*, 1957, **26**, 867–871.

52 R. A. Marcus, *J. Chem. Phys.*, 1956, **24**, 966–978.

53 F. C. Collins and G. E. Kimball, *J. Colloid Sci.*, 1949, **4**, 425–437.

54 M. v. Smoluchowski, *Z. Phys. Chem.*, 1918, **92U**, 129–168.

55 M. Dei Cas and R. Ghidoni, *Nutrients*, 2019, **11**, 2147.

56 A. Galano, *J. Mex. Chem. Soc.*, 2017, **59**, 231–262.

57 A. Galano and J. R. Alvarez-Idaboy, *J. Comput. Chem.*, 2013, **34**, 2430–2445.

58 M. Spiegel, *J. Phys. Chem. B*, 2023, **127**, 8769–8779.

59 M. Spiegel, T. Marino, M. Prejanò and N. Russo, *J. Mol. Liq.*, 2022, **366**, 120343.

60 M. Spiegel, T. Marino, M. Prejanò and N. Russo, *Phys. Chem. Chem. Phys.*, 2022, **24**, 16353–16359.

61 A. Galano and J. Raúl Alvarez-Idaboy, *Int. J. Quantum Chem.*, 2019, **119**, e25665.

62 J. M. Mayer, D. A. Hrovat, J. L. Thomas and W. T. Borden, *J. Am. Chem. Soc.*, 2002, **124**, 11142–11147.

63 M. Carreon-Gonzalez, L. Muñoz-Rugeles, A. Vivier-Bunge and J. R. Alvarez-Idaboy, *J. Comput. Chem.*, 2022, **43**, 556–567.

64 D. Q. Dao, T. C. Ngo, N. M. Thong and P. C. Nam, *J. Phys. Chem. B*, 2017, **121**, 9348–9357.

65 D. H. Truong, T. H. Lan Nguyen and D. Q. Dao, *R. Soc. Open Sci.*, 2023, **10**, 230114.

66 R. Tyburski, T. Liu, S. D. Glover and L. Hammarström, *J. Am. Chem. Soc.*, 2021, **143**, 560–576.

67 K. Milfeld, C. Guiang, S. Pamidighantam and J. Giuliani, *Cluster Computing through an Application-oriented Computational Chemistry Grid*, 2005, https://www.semanticscholar.org/paper/Cluster-Computing-through-an-Application-oriented-Milfeld-Guiang/c60eeacc596cf7a0f6c96c1362d6cc318f7dda8a.

68 R. Dooley, K. Milfeld, C. Guiang, S. Pamidighantam and D. Allen, *J. Grid Comput.*, 2006, **4**, 195–208.

69 N. Shen, Y. Fan and S. Pamidighantam, *J. Comput. Sci.*, 2014, **5**, 576–589.

70 S. Pamidighantam, S. Nakandala, E. Abeysinghe, C. Wimalasena, S. R. Yodage, S. Marru and M. Pierce, *Procedia Comput. Sci.*, 2016, **80**, 1927–1939.